Catalysis and Linear Free Energy Relationships in Aspartic Proteases†

Sinisa Bjelic and Johan Åqvist*

Department of Cell and Molecular Biology, Uppsala University Biomedical Center, Box 596, SE-751 24 Uppsala, Sweden

Received January 20, 2006; Revised Manuscript Received April 21, 2006

ABSTRACT: Aspartic proteases are receiving considerable attention as potential drug targets in several serious diseases, such as AIDS, malaria, and Alzheimer's disease. These enzymes cleave polypeptide chains, often between specific amino acid residues, but despite the common reaction mechanism, they exhibit large structural differences. Here, the catalytic mechanism of aspartic proteases plasmepsin II, cathepsin D, and HIV-1 protease is examined by computer simulations utilizing the empirical valence bond approach in combination with molecular dynamics and free energy perturbation calculations. Free energy profiles are established for four different substrates, each six amino acids long and containing hydrophobic side chains in the P1 and P1′ positions. Our simulations reproduce the catalytic effect of these enzymes, which accelerate the reaction rate by a factor of $\sim 10^{10}$ compared to that of the corresponding uncatalyzed reaction in water. The calculations elucidate the origin of the catalytic effect and allow a rationalization of the fact that, despite large structural differences between plasmepsin II/cathepsin D and HIV-1 protease, the magnitude of their rate enhancement is very similar. Amino acid residues surrounding the active site together with structurally conserved water molecules are found to play an important role in catalysis, mainly through dipolar (electrostatic) stabilization. A linear free energy relationship for the reactions in the different enzymes is established that also demonstrates the reduced reorganization energy in the enzymes compared to that in the uncatalyzed water reaction.

Aspartic proteases catalyze amide bond hydrolysis in peptides or proteins, where the substrates are either degraded for use as a nutrient source, activated to functional enzymes or building blocks, or involved in signal transduction, etc. Since the aspartic proteases comprise a large group of enzymes, they are found in all types of organisms and are not only associated with individual cells but also secreted (*1*). The catalytic aspartates are situated at the bottom of a deep cleft that is formed by two subunits or domains. Atop the cleft is a flap that closes upon binding of the substrate or inhibitor (*2*, *3*). Although a covalent type of reaction mechanism that resembles serine proteases has been proposed, the reaction mechanism that involves amide bond hydrolysis through an active site water molecule is now generally accepted. In this mechanism, one of the catalytic aspartates is protonated, while the other one is charged and functions as a general base that activates a water molecule situated in the plane formed by the carboxyl groups of the active site aspartates (*4*). The water/hydroxide ion attacks the amide bond leading to a transient tetrahedral intermediate. In subsequent reaction steps, the same aspartate, which previously functioned as a general base, acts as a general acid protonating the leaving nitrogen of the tetrahedral intermediate which leads to cleavage of the peptide bond (*5*).

The detailed protonation state of the active site aspartates has been uncertain (*4*). It is likely that a proton is initially shared between the aspartates, with the negative charge delocalized on both carboxyl moieties. However, when the substrate binds, the local symmetry is broken, causing the proton to be preferably localized on one of the catalytic aspartates, which rotates and hydrogen bonds to the carbonyl of the substrate peptide bond during the reaction (*5*). It has also been proposed that the proton transfer occurs from the protonated aspartate to the carbonyl oxygen prior to the nucleophilic attack of the water/hydroxide (*6*, *7*), generating an O-protonated amide. Amide bond hydrolysis in water may proceed through an acid-catalyzed mechanism at low pH, where a hydronium ion protonates the amide oxygen (*8*). In aspartic proteases, this would leave both aspartates charged in the proximity of each other, however, which is energetically unfavorable. Furthermore, the pK_a of the amide oxygen is approximately −1 (*9*, *10*), being approximately 6 pK_a units lower compared to that of an aspartic acid, leading to a high activation barrier for such a process. If proton transfer occurs, then it is probably taking place concomitant with or after the nucleophilic attack of the hydroxide ion (*11*, *12*). There is an additional proposed reaction mechanism that involves both outer oxygens of the aspartates in the initial step of water protolysis (*13*) but leaves the carbonyl oxygen of the scissile bond without direct stabilization (*3*).

Hence, the reaction mechanism consistent with most available data is one in which the catalytic aspartate acts as a general acid/base, by activating a water molecule and subsequently protonating the leaving nitrogen, while the other protonated Asp strongly hydrogen bonds to the developing negative charge on the substrate carbonyl oxygen. In this work, we examine the reaction energetics of this type of mechanism through extensive free energy calculations utiliz-

† Support from the Swedish Research Council (VR) and the Swedish Foundation for Strategic Research (SSF/Rapid) is gratefully acknowledged.

* To whom correspondence should be addressed. Phone: +46 18 471 4109. Fax: +46 18 53 69 71. E-mail: aqvist@xray.bmc.uu.se.

10.1021/bi060131y CCC: $33.50
Published on Web 06/03/2006

ing molecular dynamics (MD)[1] simulations in combination with free energy perturbation (FEP) and empirical valence bond (EVB) methods (*14*, *15*). Simulations are carried out for aspartic proteases plasmepsin II (Plm II), cathepsin D (Cat D), and human immunodeficiency type 1 protease (HIVP) with several different peptide substrates. Our objectives are (i) to evaluate reliable free energy profiles for the reactions, (ii) to establish the origin of catalysis in these enzymes, (iii) to explain how significantly different active sites can give rise to the same catalytic effects, and (iv) to explore whether these enzyme reactions obey linear free energy relationships as commonly observed for solution reactions.

Plasmepsins are enzymes from the malaria parasite *Plasmodium falciparum* that are involved in the initial degradation of host cell hemoglobin (*17*). Inhibitors designed against malarial plasmepsins must be selective toward human aspartic proteases to avoid serious side effects, and a human enzyme that must be considered in designing inhibitors of plasmepsins is cathepsin D (Cat D) (*18*, *19*). Human Cat D is situated in the lysosomes and is implicated in the immune response (*3*), and due to 35% sequence identity to the plasmepsins, selectivity toward it is essential for a functional drug. HIV-1 protease is involved in maturation of polyproteins and is crucial for the production of infectious virus particles (*20*), and its reaction mechanism has been the most extensively studied (*21*).

Reaction free energy profiles are calculated for the general base-catalyzed attack of the catalytic water molecule on the scissile peptide bond, yielding a (transient) tetrahedral intermediate, and for subsequent protonation and departure of the leaving nitrogen. The abstraction of the water proton by one of the catalytic aspartates is modeled as being concerted with attack of the hydroxide ion, in agreement with earlier findings that stepwise and concerted mechanisms for this reaction have similar energetics both in solution and in enzymes (*22*, *23*). Rather than C−N bond breakage, formation of the tetrahedral intermediate and proton transfers have been suggested to be rate-limiting both in solution and some proteases (*22*−*27*). As far as the aspartic proteases are concerned, the extensive studies by Meek and co-workers on HIVP have been most influential, including ^{15}N and solvent kinetic isotope effects, data on incorporation of ^{18}O into unreacted substrates, and back-reactions with peptide fragments (*6*, *28*, *29*). The inverse ^{15}N isotope effect speaks against C−N bond breakage being rate-limiting but favors nitrogen protonation. The $^{D}V/K$ solvent isotope effect of exactly 1.0 would seem to speak against a proton in flight but could mean two protons in flight; the incorporation of ^{18}O into substrate could indicate that this happens before the rate-limiting step, but since the incorporation rate is slower than the hydrolysis rate, it also seems compatible with a kinetically significant intermediate with a preceding rate-limiting barrier that is lower than that for ^{18}O exchange (which requires additional structural rearrangements). As described in ref *6*, these data do not provide a unique mechanistic solution, but the general picture emerging is that the energy barriers surrounding the tetrahedral intermediate, i.e., its formation and protonation of the leaving nitrogen, are rate-limiting and probably similar in height. This is also the conclusion that is reached herein.

The reaction mechanism and protonation states of the catalytic dyad of aspartic proteases have previously been addressed in several computational studies (*30*−*33*, *88*−*90*). These employed different approaches, ranging from gas-phase QM calculations on small model systems to QM/MM methods that treat the reacting atoms as the QM part, surrounded by enzyme and water that are represented with an MM force field. MD is often used to establish the starting configurations for different levels of QM calculations that have been used to determine activation barriers (*32*). The only work so far that has tried to evaluate free energy barriers, including the enzyme, in aspartic proteases is that of Piana et al. (*32*) on the HIV-1 protease-catalyzed peptide hydrolysis reaction. They obtained very reasonable free energy barriers of ∼20 kcal/mol and a tetrahedral intermediate at ∼12−13 kcal/mol. These calculations were, however, based on very short Car−Parrinello QM/MM trajectories of only 15 and 10 ps for the first and second reaction step, respectively, which gives relatively large uncertainties in the calculated free energies in addition to the errors associated with the choice of density functionals (BLYP) and plane wave basis sets (*32*). Furthermore, that study concluded that the enzyme electric field is anticatalytic (!), because it increases the polarity of the dielectric medium, but that protein motions are very important for the catalytic effect.

In the work presented here, we employ the EVB/MD/FEP approach that allows us to examine four different enzyme−substrate complexes and compare different aspects of catalysis. The EVB method is used to describe both the uncatalyzed solution reaction, which has been calibrated against experimental and ab initio data, and the corresponding enzyme-catalyzed reactions. The calculations generally reproduce kinetic data very well, and the generated structures are in good agreement with the three-dimensional structures of enzyme−inhibitor complexes. The question of the origin of catalysis and stabilization of the tetrahedral intermediate in these enzymes is addressed and related to structural properties. Electrostatic stabilization by prearranged dipoles plays a major role during catalysis, and not only conserved amino acid residues but also conserved water molecules, which are part of an intricate network in the enzymes, are important in both Plm II and Cat D, and in HIVP. From the calculated reaction free energy profiles, we also determine the correlation between the activation and reaction free energies, which is often denoted as a linear free energy relationship.

MATERIALS AND METHODS

The EVB scheme is used to describe amide bond cleavage by the aspartic proteases, and the reaction is represented as an interconversion between different resonance structures, Φ_i. Each resonance structure is described by a specific potential energy function, ϵ_i, that describes the bonding arrangement and charge distribution associated with that structure. The effective EVB Hamiltonian involves the diagonal (diabatic) energies of these resonance structures and off-diagonal terms that describe the mixing between the

[1] Abbreviations: Plm II, plasmepsin; Cat D, cathepsin D; HIVP, human immunodeficiency type 1 protease; MD, molecular dynamics; FEP, free energy perturbation; EVB, empirical valence bond; TI, tetrahedral intermediate; TS, transition state.

states. Each diagonal energy function is given by

$$H_{ii} = \epsilon_i = U^{(i)}_{\text{bond}} + U^{(i)}_{\text{angle}} + U^{(i)}_{\text{torsion}} + U^{(i)}_{\text{nb,rr}} + U^{(i)}_{\text{nb,rs}} + U_{\text{ss}} + \alpha^{(i)} \quad (1)$$

where the first three terms describe the intramolecular potential energies of the reacting fragments (and their possible connections across the QM/MM boundary) by Morse bond potentials, harmonic three-atom angle bending, and proper and improper torsional angle functions. The fourth term denotes nonbonded van der Waals and electrostatic interactions within and between the reacting fragments. The fifth and sixth terms describe the interactions between the reactants and the surrounding environment and the potential energy of the surrounding enzyme/water system, respectively, in terms of a standard force field. The last term of the Hamiltonian represents the intrinsic gas-phase energy of the given resonance structure with all fragments at infinite separation, i.e., noninteracting (*14*, *15*).

Combination of the EVB representation of the reaction potential surface with the MD/FEP technique allows us to drive the system between valence bond states *i* and *j* and sample system configurations along the way (*14*, *15*). At each configuration, the ground-state energy is obained as the lowest eigenvalue of the secular equation. Besides the diagonal (diabatic) energies, the ground state also depends on the off-diagonal matrix elements, H_{ij}, representing the adiabatic mixing of the VB states and is typically described by an exponential function or a constant (*14*, *15*, *23*, *34*). The EVB potential surface is fitted to available experimental or ab initio data regarding the uncatalyzed reaction in solution by adjusting the off-diagonal terms as well as the gas-phase energy shifts, $\alpha^{(i)}$ (*14*, *15*). The solution free energy surface is thus calibrated, and the parameters $\alpha^{(i)}$ and H_{ij}, although they in principle pertain to the gas-phase surface, are not explicitly parametrized for the gas-phase reaction. The advantage with this approach is that possible errors in the solvation free energies (that relate the gas-phase reaction to the energetics in solution) of the reaction fragments can be handled by the calibration. This is useful since an accurate gas-phase parametrization could easily be "destroyed" by errors in the reactant and product solvation energies of a few kilocalories per mole, thereby rendering the resulting solution surface much less accurate.

The calculations of free energy profiles follow the FEP procedure described in refs *14* and *15*. For the transformation between the VB states in a two-state model, the initial and final states are "connected" via a set of intermediate mapping potentials ($\epsilon_m = \lambda_1{}^m\epsilon_1 + \lambda_2{}^m\epsilon_2$, where ϵ_i is given by eq 1 and $\lambda_1{}^m + \lambda_2{}^m = 1$). The mapping vector $\vec{\lambda}_m = (\lambda_1{}^m,\lambda_2{}^m)$, defining a linear combination between the potentials, changes between values (1,0) for reactants and (0,1) for products. The free energy associated with moving from the initial to final potential in *n* discrete steps is obtained from Zwanzig's formula (*35*)

$$\Delta G(\vec{\lambda}_n) = \Delta G(\vec{\lambda}_0 \rightarrow \vec{\lambda}_n) = -\beta^{-1}\sum_{m=0}^{n-1} \ln\langle \exp[-\beta(\epsilon_{m+1} - \epsilon_m)]\rangle_m \quad (2)$$

where $\beta = 1/kT$ and the average $\langle\ \rangle_m$ is evaluated on the mapping potential surface ϵ_m. The free energy profile $\Delta G(X)$ corresponding to trajectories moving on the actual ground-state potential, $E_g(X)$, is calculated from the umbrella sampling expression (*34*)

$$\Delta G(X_n) = \sum_{m\supset\Delta\epsilon=X_n} w_m(\Delta G(\vec{\lambda}_m) - RT \ln\langle \exp\{-[E_g(X_n) - \epsilon_m(X_n)]/RT\}\rangle_m)/\sum_{m\supset\Delta\epsilon=X_n} w_m \quad (3)$$

where the discretized reaction coordinate ($X_n = \Delta\epsilon = \epsilon_1 - \epsilon_2$) is the energy gap between the initial and final diabatic surfaces (*14*, *15*, *34*). Different mapping vectors contribute to the reaction coordinate interval X_n and are weighted proportionally to the total contribution in that interval, namely, $w_m/\sum w_m$. Ground-state energy $E_g(X_n)$ is obtained by mixing the diabatic states, ϵ_i, yielding the secular equation with solution

$$E_g = \frac{1}{2}(\epsilon_i + \epsilon_j) - \frac{1}{2}[(\epsilon_i - \epsilon_j)^2 + 4H_{ij}{}^2]^{1/2} \quad (4)$$

The initial general base abstraction of the water proton by the catalytic aspartate and the following nucleophilic attack of the hydroxide ion on the scissile peptide bond can be represented by three different resonance structures (Scheme 1) as used in our earlier calculations on the histo-aspartic protease (HAP) from *P. falciparum* (*23*). Φ_1 is the resonance form for the reactants, and Φ_3 represents the tetrahedral intermediate resulting from the nucleophilic attack of the hydroxide ion. The reaction proceeding from Φ_1 to Φ_3 is either stepwise, i.e., Φ_2 is fully formed, or concerted. Here, only the concerted reaction mechanism is considered since our earlier calculations for the malarial HAP enzyme showed that the barriers on the free energy surface are similar for the concerted and stepwise pathways (*23*). It has also been found that the trypsin reaction as well as the uncatalyzed hydrolysis of formamide has similar activation energies for the concerted and stepwise mechanisms, implying a flat transition-state surface (*22*). The following protonation of the leaving nitrogen and C−N bond breakage are represented by moving from Φ_3 to Φ_4 and from Φ_4 to Φ_5, respectively, and are simulated in the same manner as the first reaction step ($\Phi_1 \rightarrow \Phi_3$).

The advantage of the EVB method is that, by simulating peptide bond hydrolysis in water without the enzyme present, we are able to calibrate the water reaction and activation free energies to reproduce experimental and ab initio results from refs *22* and *36*−*39* by adjusting the EVB parameters [$\Delta\alpha_{ij} = \alpha^{(j)} - \alpha^{(i)}$ and H_{ij}]. The overall activation energy for the tetrahedral intermediate formation ($\Phi_1 \rightarrow \Phi_3$) is 33 kcal/mol, and the energy difference between Φ_3 and Φ_1 is 27 kcal/mol (*23*). It can be divided into proton transfer from water to the aspartate side chain ($\Phi_1 \rightarrow \Phi_2$), with a free energy difference of 15 kcal/mol and a barrier height of 18 kcal/mol (*36*, *38*), and hydroxide ion attack on the peptide bond ($\Phi_2 \rightarrow \Phi_3$), with a corresponding activation barrier of 18 kcal/mol and a free energy difference of 12 kcal/mol (*22*, *37*, *39*). The proton transfer from an aspartic acid residue to a secondary amine nitrogen ($\Phi_3 \rightarrow \Phi_4$) has an activation barrier of ∼2 kcal/mol and a free energy difference of −5 kcal/mol (*23*). Thus, the overall uncatalyzed reaction $\Phi_1 \rightarrow$

Scheme 1: Resonance Structures (Φ_i) Used in the EVB Calculations

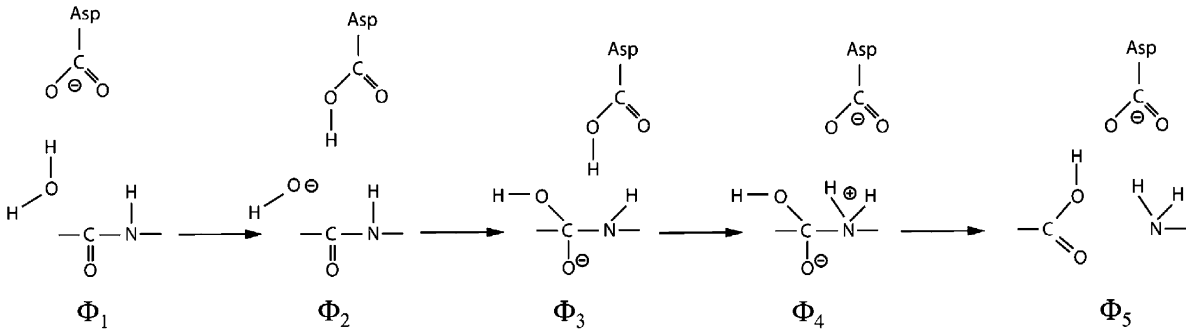

Table 1: Enzymes and Corresponding Substrates Used in the Calculations

enzyme	substrate
plasmepsin II[a]	Arg-Met-Phe-Leu-Ser-Phe
cathepsin D[b]	Ile-Ala-Phe-Phe-Ser-Arg
HIV-1 protease[c]	Lys-Ile-Leu-Phe-Leu-Asp
HIV-1 protease[c]	Gln-Val-Leu-Ala-Ile-Ala

[a] From ref *40*. [b] From ref *41*. [c] From ref *42*.

Φ_4 has estimated activation and reaction free energies of 33 and 22 kcal/mol, respectively. The C−N bond dissociation was parametrized as in ref *23*. When necessary, the correction for bringing the reactants from a 1 M standard state into a solvent cage with the same concentration as surrounding water (55 M) has been made (*14*).

The tetrahedral intermediates (TIs) were built and docked manually on peptidic inhibitors in the enzyme crystal structures of Plm II, Cat D, and HIVP with PDB entries 1LEE (*40*), 1LYB (*41*), and 4HVP (*42*), respectively (Table 1). Substrates were chosen so that hydrophobic residues were in the P1 and P1′ positions and experimentally derived free energies of activation were at least 10 kcal/mol lower compared to those of the uncatalyzed reaction (*43*−*46*). A simulation sphere with a diameter of 44 Å was centered on the outer oxygen of the general acid/base aspartate, and the system was solvated with TIP3P water molecules (*47*). In total, 482, 452, 678 (K-I-L-F-L-D substrate), and 685 (Q-V-L-A-I-A substrate) water molecules were added to 1LEE (*40*), 1LYB (*41*), and 4HVP (*42*), respectively. The negatively charged catalytic aspartates are Asp214 in Plm II, Asp231 in Cat D, and Asp25′ in HIVP. It can also be noted that Asp303 in Plm II and Asp323 in Cat D have one of their side chain oxygens only 2.6 Å from the carbonyl oxygen of Ser215 and Thr232, respectively, and these Asp's were therefore protonated. Crystallographic water molecules were discarded with the exception of HOH511 in 4HVP, which is positioned between the flap region and the inhibitor (*42*), and the catalytic water was in each case inserted into the crystal structures at the position corresponding to the relevant tetrahedral intermediate oxygen.

All MD/FEP/EVB calculations were performed with Q (*48*) utilizing the OPLS-AA force field (*49*). We equilibrated the solvated enzyme−substrate complexes by slow heating from 1 to 300 K for 380−740 ps and increasing the time step from 0.01 to 1 fs. Free energy perturbation calculations for each reaction step were carried out with 41 values of the mapping parameter λ, with a 4 ps trajectory calculated at each point out of which 87% was used for data collection. No cutoff was used for the nonbonded interactions between atoms involved in the reaction and the surroundings. Other atoms were subjected to a nonbonded cutoff of 10 Å, and electrostatic interactions beyond 10 Å were treated with the local reaction field (LRF) method to take into the account long-range effects (*50*). Water molecules close to the sphere surface were subjected to radial and polarization restraints (*48*, *51*). All atoms outside the water sphere were held by harmonic positional restraints of 100 kcal mol^{-1} Å^{-2}, and their nonbonded interactions are excluded. Water bonds and angles were constrained with the SHAKE procedure (*52*). Charges for the tetrahedral intermediate are the same as in ref *23*. Simulations of uncatalyzed peptide hydrolysis in water were carried out with the same FEP/EVB protocol, and the reference reaction was calibrated to reproduce experimental and ab initio results (*22*, *36*−*39*) as described above. All FEP calculations were initiated at the TI and carried out toward the reactants and products to achieve the most efficient configurational sampling. The values of $\Delta\alpha_{1\rightarrow3}$ and H_{13} obtained for the uncatalyzed water reaction are 155 and 116 kcal/mol, respectively. For the next reaction step, leading from Φ_3 to Φ_4 and from Φ_4 to Φ_5, the calibrated values are as follows: $\Delta\alpha_{1\rightarrow4} = 115$ kcal/mol and $H_{34} = 79$ kcal/mol and $\Delta\alpha_{1\rightarrow5} = -128$ kcal/mol and $H_{45} = 61$ kcal/mol, respectively. This calibration is then used without any change for the different enzyme reactions and is in agreement with our previous study of the histo-aspartic protease (*23*). Moreover, the calibration of the concerted TI formation was also validated on the Ala-Ala dipeptide (MeCO-Ala-Ala-NHMe) following the protocol in ref *23* and by extending the FEP procedure to 101 λ points each with 10 ps sampling.

RESULTS AND DISCUSSION

Aspartic proteases are efficient catalysts of peptide degradation and are experimentally found to accelerate the reaction by ∼10^8−10^{12}-fold, depending on the substrate (*17*, *43*−*46*, *53*), compared to the corresponding reaction in water which is extremely slow, ∼10^{-11} s^{-1} (*22*, *36*−*39*). Calculated free energy profiles in the different enzymes are presented in Figure 1, where the calibrated uncatalyzed reaction profile in water is also shown. For Plm II and HIVP (K-I-L-F-L-D substrate), both the nucleophilic attack and nitrogen protonation and departure steps are calculated (Figure 1A,C). It can be seen that the two transition states before and after the tetrahedral intermediate are very similar in height and that the entire region around the TI is rather flat. This may, of course, complicate the interpretation of isotope effect measurements since several molecular species then could contribute to the observed rates. Here, we will mainly focus on the structure and energetics of the TI region, and for the

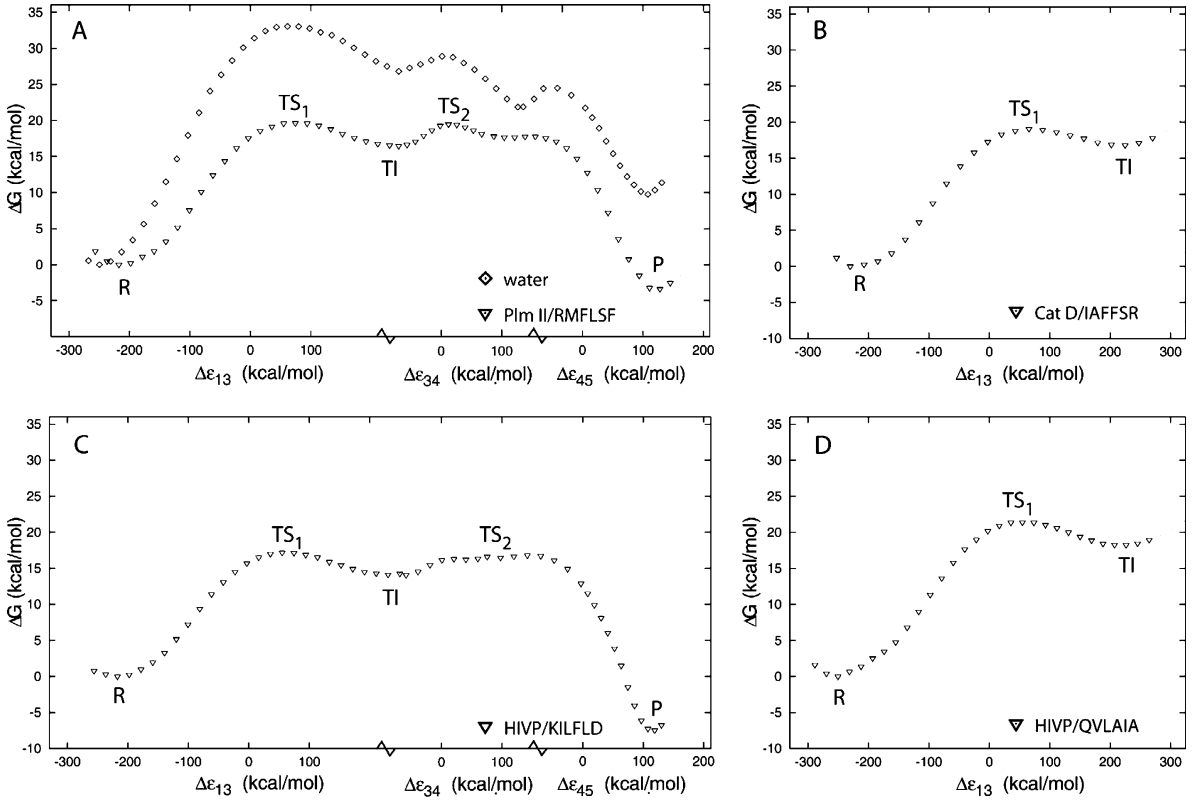

FIGURE 1: Free energy profiles for the water reaction and for the enzyme-catalyzed hydrolysis of peptides: (A) Plm II/R-M-F-L-S-F (▽) and water reaction (◇), (B) Cat D/I-A-F-F-S-R, (C) HIVP/K-I-L-F-L-D, and (D) HIVP/Q-V-L-A-I-A. In panels A and C, the entire reaction from Φ_1 to Φ_5 is presented, whereas in panels B and D, only the path from Φ_1 to Φ_3 is shown. $\Delta\epsilon$ is the generalized reaction coordinate corresponding to the energy gap between the indicated states. P, R, TS, and TI denote products, reactants, transition state, and tetrahedral intermediate, respectively.

Table 2: Observed and Calculated Activation and Reaction Free Energies (in kilocalories per mole relative to Φ_1)

substrate system	$\Delta G_{obs}^{\ddagger}$	$\Delta G_{calc}^{\ddagger}(\Phi_1 \rightarrow \Phi_3)$	$\Delta G_{calc}^{0}(\Phi_1 \rightarrow \Phi_3)$	$\Delta G_{calc}^{\ddagger}(\Phi_3 \rightarrow \Phi_4)$	$\Delta G_{calc}^{\ddagger}(\Phi_5 \rightarrow \Phi_6)$	substrate
plasmepsin II	17.6[a]	19.6	16.5	19.6	17.9	R-M-F-L-S-F
cathepsin D	15.9[b]	19.1	16.8	−	−	I-A-F-F-S-R
HIV-1 protease	17.6[c]	17.2	14.1	16.4	16.6	K-I-L-F-L-D
HIV-1 protease	21.0[d]	21.4	18.3	−	−	Q-V-L-A-I-A
HAP[e]	19[f]	20[g]	12[g]	13[g]	10[g]	R-M-F-L-S-F
water[h]	33	33	27	29	25	dipeptide

[a] From ref *46*; alternatively values of 16.1 from ref *17* and 17.00 from ref *53*. [b] From ref *45*. [c] From ref *43*. [d] From ref *44*. [e] Histo-aspartic protease. [f] From ref *17*. [g] From ref *23*. [h] See Materials and Methods.

reaction with Cat D and the second HIVP substrate, only the formation of the tetrahedral intermediate is considered.

It can immediately be seen that all three enzymes exert a large catalytic effect on the reaction, especially reflected as a stabilization of the TI and the preceding transition state (TS) that has to be crossed. This TS is stabilized by 12−16 kcal/mol, while the free energy of the TI is lowered by 9−13 kcal/mol in the different enzymes. The transition state associated with nucleophilic attack in the aspartic proteases is located relatively close to the TI; it is thus a late TS and is mainly sampled with the FEP mapping parameters, $\vec{\lambda}_m =$ (0.375,0.625). The same picture is obtained from the average EVB coefficients for ground-state energy E_g in the TS ensemble of structures, which gives between 61 and 65% weight to the TI resonance form for the different enzymes. This is, of course, in agreement with the Hammond postulate for an endothermic reaction. It is, however, noteworthy that both the EVB coefficients and the location of the TS along the generalized reaction coordinate are very similar in all enzymes, indicating that the structure and charge distribution of the TS are robust features of these aspartic proteases. That the EVB coefficients in general can change substantially depending on the environment is discussed elsewhere (e.g., ref *54*).

The individual TS and TI free energies relative to the reactants are given in Table 2 for the different reactions, where also results from recent simulations of HAP (histo-aspartic protease) from *P. falciparum* are shown for comparison (that enzyme has one of the catalytic aspartic acids mutated to a histidine, which makes it particularly interesting) (*17*, *23*). Furthermore, in the case of Plm II and HIVP (K-I-L-F-L-D substrate), we also evaluated the free energy profiles for C−N bond breakage following the procedure in ref *23*, and the barrier for this process was indeed found to be lower than that for the initial nucleophilic attack on the peptide bond, with calculated values of 17.9 and 16.6 kcal/mol for Plm II and HIVP, respectively (Table 2). In general, the calculated activation free energies are in remarkably good agreement with experimental ones derived from transition-state theory. The only deviation from experiment larger than 2 kcal/mol is for Cat D where the barrier is overestimated

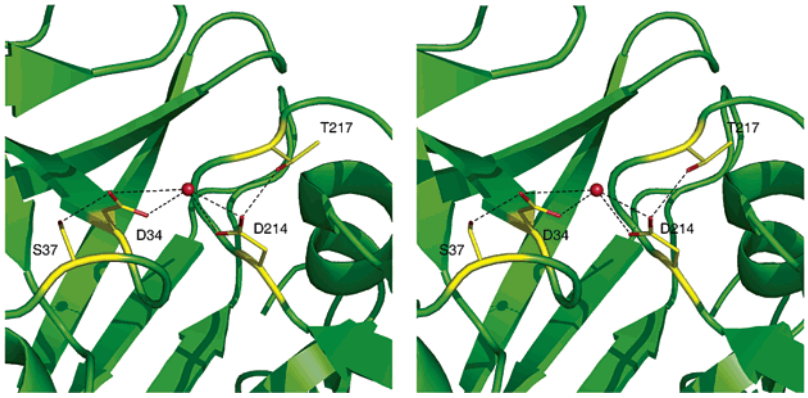

FIGURE 2: Interaction between the central water molecule and catalytic residues in the crystal structure of Plm II (*87*). Outer oxygens of the aspartates are within hydrogen bonding distance of the threonine and serine residues.

by ~3 kcal/mol, and we will return to this issue below. The errors in the calculated free energies in Table 2 can be estimated as a sum of the forward and backward summation error associated with the free energy perturbation calculations and the error associated with using different initial conditions. The latter was assessed by starting the EVB sampling from random points along the initial equilibration trajectories. Using this procedure, one obtains total statistical error estimates between 0.9 and 2.0 kcal/mol, with an average error of approximately 1.5 kcal/mol. It is thus clear that the stabilization of the transition states relative to the water reaction is much larger than the corresponding errors. Taken together, the five different enzyme calculations in Table 2 clearly demonstrate that the EVB model is able to capture the catalytic effect of aspartic proteases accurately and that there is a significant stabilization of the TI accompanying the reduced activation free energy. It can be noted here that the substrates are built from the inhibitors in the existing crystal three-dimensional structures, with the exception of HAP (*23*), and no major adjustments were required to fit the active sites. With the high degree of structural similarity between substrates and inhibitors, automated docking calculations, like those used in the HAP case (*23*), are not necessarily required for the prediction of substrate conformations.

The main structural differences among Plm II, Cat D, and HIV-1 protease are (i) the flap region that in HIVP consists of two flaps, (ii) the consensus Asp-Thr/Ser-Gly (*3*) sequence of aspartic proteases which continues with alanine in HIVP (in Plm II and Cat D it is either a serine or threonine), and (iii) the counterpart of Tyr77 (Plm II numbering) in the flap that has also been implicated in TS stabilization (*55*) but is not present in HIVP. The substrate is held in position during the reaction by a hydrogen bond network between the backbone of the substrate and the enzymes, as well as by the complementary shape of the substrate and the active sites. Being a homodimer, HIVP totally enfolds the substrate, while Plm II with only one flap exposes a greater part of the active site to water. This may be one reasone for why additional interactions between Ser37 and Thr217 (Plm II numbering) and the catalytic aspartates in Plm II and Cat D are required (Figure 2).

The initial protonation of the aspartates has been disputed, but the model described herein is supported by several studies (*5*, *11*, *12*, *30*, *32*), although models in which the opposite aspartate is protonated have also been reported (*56*, *57*). Before substrate binding, the aspartates are most likely sharing a proton, which is supported by MD simulations of the apoenzymes (data not shown), and the monoprotonated form of the catalytic dyad is part of a pH-dependent equilibrium with the enzyme in both diprotonated and ionized forms (*58*). After the substrate binds, a rearrangement of the aspartates takes place during the reaction, enabling the protonated Asp to make a strong hydrogen bond to the developing negative charge on the substrate carbonyl. Since the peptide is in an extended form with the carbonyl of the scissile bond positioned directly above the protonated aspartate, it is possible for the charged aspartate to activate the catalytic water. This is in accordance with previous theoretical studies (*32*) in which the hydrogen-bonded catalytic aspartates in the reactant state are found to have a lower energy than when an outer oxygen is protonated. That there occurs an isomerization step in the enzyme prior to substrate hydrolysis, where the enzyme is isomerized to a kinetically competent complex, has also been found in the work of Porter et al. (*59*). The simulated substrates are generally two amino acids shorter than the ones used in the kinetic assays (*43*−*46*), not taking into the account the linked fluorophore and quenching groups in Plm II and Cat D. The corresponding effects on the relative rates between the enzymes should, however, not be very pronounced and are <1 kcal/mol for Plm II and Cat D (*45*, *46*). The obtained rate constants for Plm II and Cat D are somewhat underestimated compared to the experimental rates but are still in reasonable agreement, whereas they are reproduced very well for HIVP.

The structure of the TI that emerges from the MD simulations (Figure 3) closely resembles the transition-state mimics present in crystallographic complexes with enzymes (*40*−*42*). It is clearly evident from Figure 3 that the TI has surprisingly similar conformations in both Plm II/Cat D and HIVP. Notably, most important hydrogen bonding interactions are centered around the scissile bond. The aspartate that is initially protonated donates, as expected, a very strong hydrogen bond to the anionic oxygen of the TI, and this proton may well be transiently transferred to the TI in accordance with some mechanistic proposals (*7*, *11*, *12*). Although such a resonance structure could also be included in our calculations, it appears that the situation is represented well by a strong anionic hydrogen bond, which will also be present if the proton is formally located on the TI oxygen. The structures and activation energies determined here also

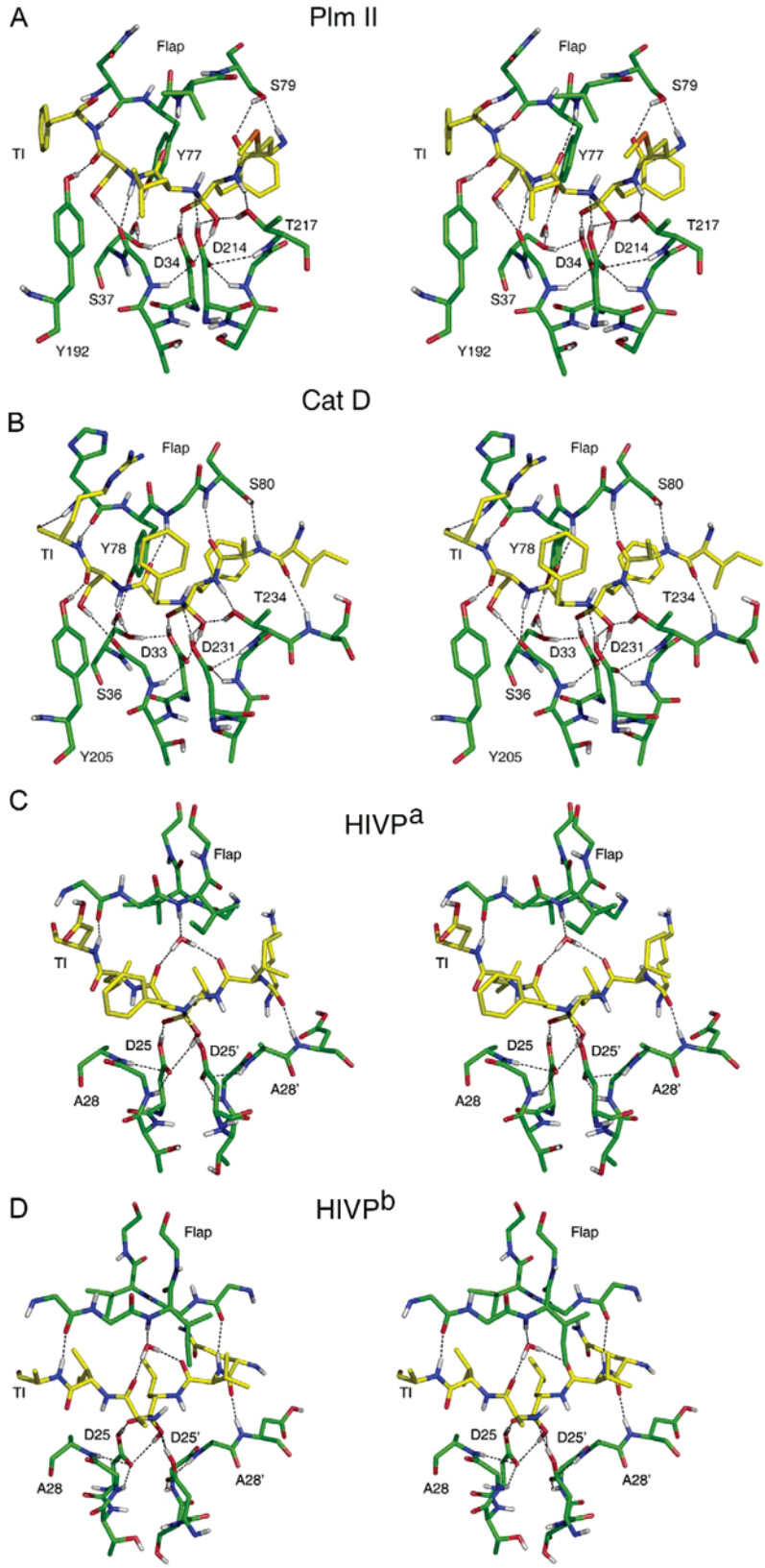

FIGURE 3: Tetrahedral intermediate (yellow) in complex with the respective enzyme (green): (A) Plm II/R-M-F-L-S-F, (B) Cat D/I-A-F-F-S-R, (C) HIVP[a] in complex with K-I-L-F-L-D, and (D) HIVP[b] in complex with Q-V-L-A-I-A.

agree well with QM/MM calculations on HIVP (*30*, *32*), but it can be noted that hydrogen bonding between the general base aspartic acid and the leaving nitrogen is not predicted in the TI of ref *32*. In our simulations, the general base aspartic acid in all cases has its proton interacting with both the leaving nitrogen and the hydroxyl group of the TI, indicating that the substrate is in a perfect conformation for catalysis. In fact, hydrogen bonding to the leaving nitrogen in the tetrahedral intermediate could already contribute to an observed inverse ^{15}N kinetic isotope effect, making the assignment of nitrogen protonation as the rate-limiting step less certain. This issue was checked by calculating the

equilibrium ^{15}N isotope effect upon formation of a hydrogen bond between CH_3OH and NH_2CH_3 or $NH(CH_3)_2$ at the HF/6-31G* level using the Bigeleisen equation (*60*) and following the procedures in refs *61* and *62*. The resulting isotope effect is as expected inverse and ~0.998. It thus seems possible that the observed ^{15}N kinetic isotope effect of 0.995 (*6*, *28*, *29*) could reflect just hydrogen bonding rather than full proton transfer to the leaving group.

The substrate conformation farther from the cleaved peptide bond is also predicted to interact favorably with specific hydrogen bonds to the enzyme. For instance, the substrate P2 and P1′ carbonyls are accepting hydrogen bonds in Plm II/Cat D from the flap and in HIVP from the water molecule situated between the flaps and the substrate. Although it is more difficult to predict binding conformations near the ends of the substrate, where the active site funnel broadens, the interaction between the substrate and Ser79 (Plm II) and Ser80 (Cat D) is properly reproduced. This interaction has been shown to be important for catalysis, and the loss of it has an negative effect on the rate constant (*63*).

Detailed analysis of the active site residues reveals that the geometries of the catalytic dyad and the TI are exceptionally similar in HIVP, Plm II, and Cat D. The groups surrounding the catalytic aspartates, which have the same function in both types of aspartic proteases, are the backbone nitrogens of Gly36 and Gly216 in Plm II and Gly27 and Gly27′ in HIVP (Figure 3). Immediately noticeable in HIVP is the lack of serine or threonine residues that interact with the outer oxygen of Asp25 and the hydroxyl of the TI as in Plm II or Cat D. These residues are replaced with Ala28 and Ala28′ in HIVP, which are both involved in stabilization of the inner oxygens of Asp25 and Asp25′ by backbone nitrogens. Overall, the protonated aspartate in HIVP loses a hydrogen bond interaction, present between Ser37 O_γ and Asp214 $O_{\delta1}$ in Plm II and respective residues in Cat D, but gains an alternative interaction with Ala28 N. However, there is no obvious replacement in HIVP for the Plm II Thr217 interaction that is involved in TI stabilization (the energetics behind this is discussed in the next section). The role of this side chain seems puzzling since it is changed to an alanine in renin (*64*), a Plm II-like protease, without a loss of catalysis. As discussed by Andreeva and Rumsh (*65*), the presence of this residue is correlated with pH, and in enzymes working at high acidity, it is essential for protecting the charge on the catalytic aspartate. Since HIVP catalyzes peptide hydrolysis at a pH optimum of 6 (*58*), the presence of the threonine residue may not be required. However, it seems to be necessary in Plm II that is involved in hemoglobin degradation in the acidic food vacuole of the parasite, with a pH of ~5, which is also the pH optimum of the enzyme (*66*). Cat D purified from human erythrocytes also has an activity maximum at an acidic pH of ~3 (*67*), and the presence of the corresponding Thr234 thus appears logical (cf. Figure 3A,B).

The aspartic proteases considered here are good examples of how enzymes use their three-dimensional network of amino acids, not only to provide a stable frame for the stabilization of the transition state but also for incorporating water molecules that conserve structural features or direct their dipoles for favorable interactions during the reaction. In Plm II, there are two water molecules involved in the positioning of side chains, wat1 and wat2, that are conserved during MD and are bridging the electrostatic interactions between Tyr77 O_η, Ser37 O_γ, and Asn39 O (wat1) and the substrate Ser O_γ, Ala38 N, and Leu131 O (wat2), respectively (Figure 4). It is remarkable that the MD simulations are able to predict the position of these water molecules, especially taking into the account the fact that no crystallographic waters, except the catalytic one, are retained from the X-ray structures. It was demonstrated previously that wat1 is conserved across pepsin-like aspartic proteases and possibly important for the reaction mechanism (*65*). The proposed hydrogen bond pattern with respect to the TI and wat1 in ref *65* is reproduced by our simulation and is unchanged during catalysis. On the other hand, it appears that wat2 is only present in those cases in which the P2′ position in the substrate is a serine residue.

In HIVP, water molecules appear to play a more important role in stabilizing the tetrahedral intermediate by favorably oriented dipoles. The interaction energy between the structurally conserved HIVP water molecule (wat1), situated between the flap region and the TI, and the reacting groups in the EVB region is calculated to be −4.4 kcal/mol. In addition to wat1, we found four other water molecules, wat2−5 (Figure 4), that contribute significantly to the interactions with the reacting system, approximately −8 kcal/mol. As illustrated in Figure 5, where the distribution of water molecules is plotted in terms of their interaction energy with the TI, wat1−5 are unique relative to the rest of the water molecules that mainly have energies between −1 and 1 kcal/mol. Like wat1, wat2−5 also have their dipoles pointing with their positive ends toward the TI (Figure 4). In total, these five water molecules (wat1−5) contribute approximately −12 kcal/mol to the electrostatic interactions with the reacting system in the TI, with both substrates. Wat1 has the largest contribution as expected. Furthermore, it is notable that the five water molecules are conserved in the wild type as well as different mutants of HIVP (*68*), and their predicted positions are compared in Figure 4 to the crystallographic ones (*68*). It should again be emphasized that wat2−5 were not retained from the crystal structure but evidently find their way into the favored positions spontaneously, and it is striking how well the MD simulations are able to predict the microscopic picture a priori. In the HIVP complex with the Q-V-L-A-I-A substrate, having an alanine in the P1′ position, two additional water molecules can enter the space that is occupied by the phenylalanine in the K-I-L-F-L-D substrate. This results in a less organized enzyme−substrate structure on the prime side that seems to explain the much slower catalytic rate for the Q-V-L-A-I-A substrate.

Origin of the Catalytic Effect in Aspartic Proteases. The catalytic power of the aspartic proteases is analyzed here by comparing average intra- and intermolecular interactions involving the EVB region and the surroundings, both in water and in the enzyme reactions. In water, solvent-induced barriers may arise due to the delocalization of charge in the transition state or high-energy intermediates. The attack of hydroxide ion on formamide is an example in which the resulting TI is significantly destabilized by solvation effects as the concentrated hydroxide charge becomes spread out over several atoms (*22*, *69*). This type of effect also contributes to the destabilization of the tetrahedral intermediate in water compared to the enzymes in the present case, where the negative charge initially resides on a carboxylate

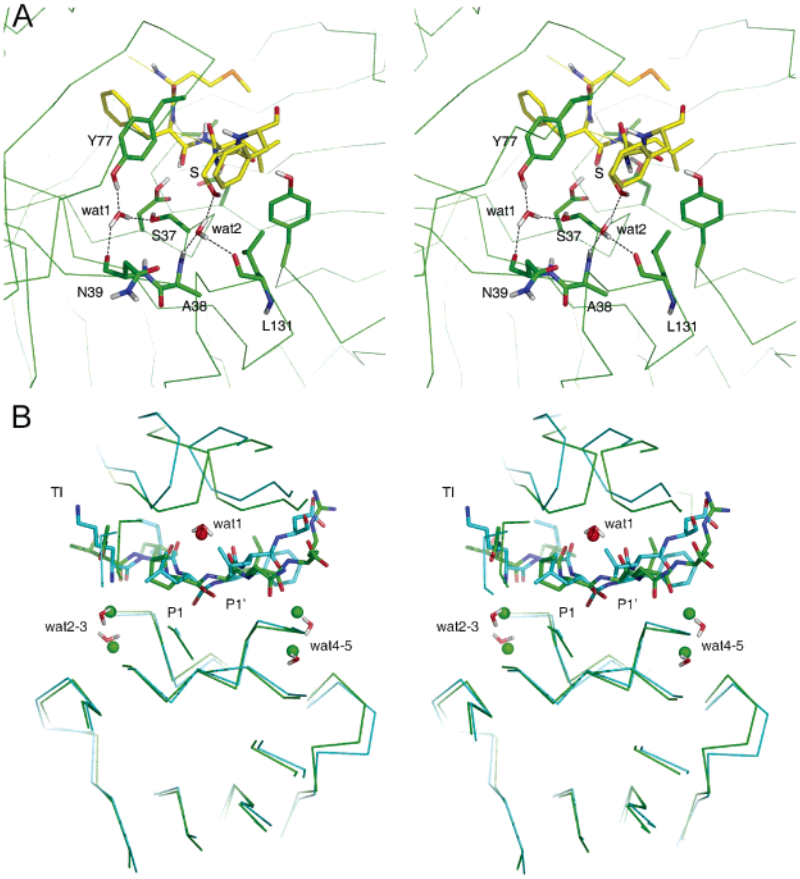

FIGURE 4: Positions of important water molecules in the MD simulation: (A) Plm II and (B) HIVP/K-I-L-F-L-D. The structure of HIVP in complex with the TI is superimposed on X-ray structure 1FFI. Green spheres are water molecules from the crystal structure and have been found to be conserved (*68*).

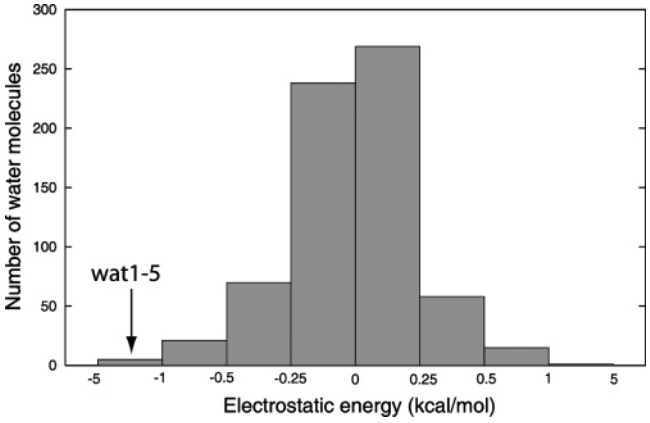

FIGURE 5: Distribution of the water molecules in HIVP/K-I-L-F-L-D at the TI state as a function of electrostatic energy between the water molecules and the reacting system. Wat1−5 have energies in the range of −5 to −1 kcal/mol.

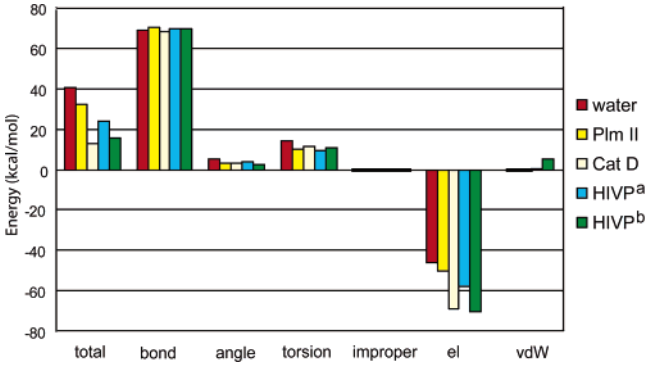

FIGURE 6: Energy difference between the TI and the reactants in water and in the enzymes. The calculated energies are only for the groups in the EVB region. Abbreviations: el, electrostatic energy; vdW, van der Waals energy. HIVP is in complex with the K-I-L-F-L-D substrate. HIVP is in complex with the Q-V-L-A-I-A substrate.

group (*23*). The contribution from the bonded energy terms and the nonbonded van der Waals interactions do not have any significant effect on catalysis, while a general trend of more favorable electrostatic interaction in the enzymes than in solution is observed (Figure 6). The most prominent contributions to the electrostatic interaction energy with the reacting groups are naturally associated with residues centered around catalytic aspartates. However, there are also significant contributions from groups localized farther from the aspartates (Figures 7 and 8), including the HIVP water molecules mentioned above (Figures 4 and 5). Residues that have interaction energies below approximately −5 kcal/mol are in Plm II (Cat D), besides the catalytic aspartates, Gly36 (Gly35), Tyr77 (Tyr78), Tyr192 (Tyr205), Gly216 (Gly233), and Thr217 (Thr234) (Figure 7). The favorable energies mainly reflect interactions with the negative charge that, after water proton abstraction by the catalytic aspartate, is migrating to the tetrahedral intermediate. The backbone NH groups of Gly216 and Gly36 are donating hydrogen bonds to the oxygens of the aspartates. During the simulations, Thr217 $O_{\gamma 1}$ is positioned equidistantly between Asp214 $O_{\delta 1}$ and the TI in Plm II and is directly involved in stabilizing the reaction (Figure 3). Asp34 (Asp33) in Plm II (Cat D) is providing the main stabilization of the negatively charged oxygen in

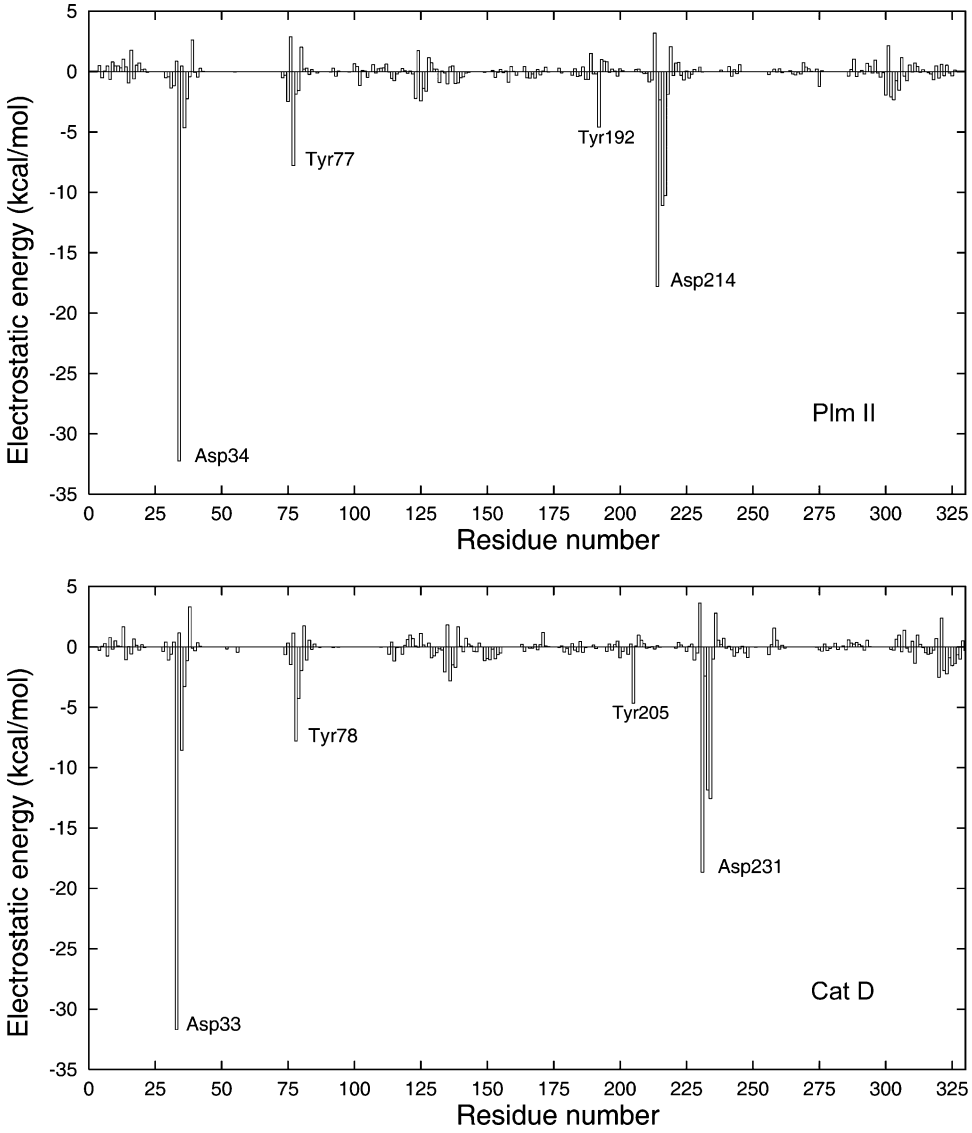

FIGURE 7: Electrostatic interactions between the residues in Plm II (top) and Cat D (bottom), and the reacting system used in the EVB calculations at the TI state.

the TI, but another residue that is relatively close is the aromatic ring of Tyr77, with a shortest distance of 4 Å. In aspartic proteases, it has been implied that the edge of the aromatic ring of the counterpart of Tyr77 contributes to the stabilization of the developing negative charge on the substrate oxygen (*55*). Tyr77 in Plm II contributes ca. −8 kcal/mol to electrostatic interaction with the reacting groups at the TI, approximately half coming from the backbone with the rest from the side chain. The orientation of the tyrosine ring as well as the distance to the negative oxygen determines the magnitude of the interaction, which in our case is ca. −3.5 kcal/mol. This type of oxygen−aromatic ring interaction in proteins has been discussed in detail previously (*70*). The mutation of the equivalent tyrosine to phenylalanine, Tyr75Phe, in pepsin does not result in any major decrease in k_{cat} (*71*). On the contrary, mutations to other amino acids, except for asparagine, lead to a much lower activity, and these findings thus support the role of favorable aromatic ring interactions with the TI (*71*). Tyr192 in Plm II also has a favorable electrostatic interaction energy with the reacting species, and as for Tyr77, the side chain contributes approximately half, i.e., −2 kcal/mol, of the total −4.6 kcal/mol interaction. The situation is equivalent in Cat D, and it is clearly evident from Figure 7 that these two tyrosines, not present in HIVP, make a greater contribution during the reaction than most of the other amino acids.

The plots of the electrostatic interaction energy between the TI and the surrounding protein residues in HIVP are remarkably similar to those of Plm II and Cat D around the catalytic aspartates (Figures 7 and 8). However, there are differences involving Gly27 and Gly27′, and Ala28 and Ala28′, in HIVP. Gly27′ is the counterpart of Gly216 (Gly233) in Plm II (Cat D) and has approximately the same interaction energy with the reacting groups, while Gly27 stabilizes the reacting species more in HIVP than does the Plm II (Cat D) Gly36 (Gly35) residue. Ala28 is energetically equal to Ser37 (Ser36), while Ala28′ is clearly not able to replace the effect of Thr217 (Thr234) in Plm II (Cat D). Therefore, our conclusion is that the favorable interaction between Thr217 (Thr234) and the EVB region in Plm II (Cat D) is counterbalanced by the strong Gly27 interaction in HIVP. Another striking difference is the lack of tyrosine residues Tyr77 (Tyr78) and Tyr192 (Tyr205) present in Plm II (Cat D), but as mentioned previously, HIVP has two flaps and several structurally conserved water molecules that can compensate for these interactions. We note that neither our

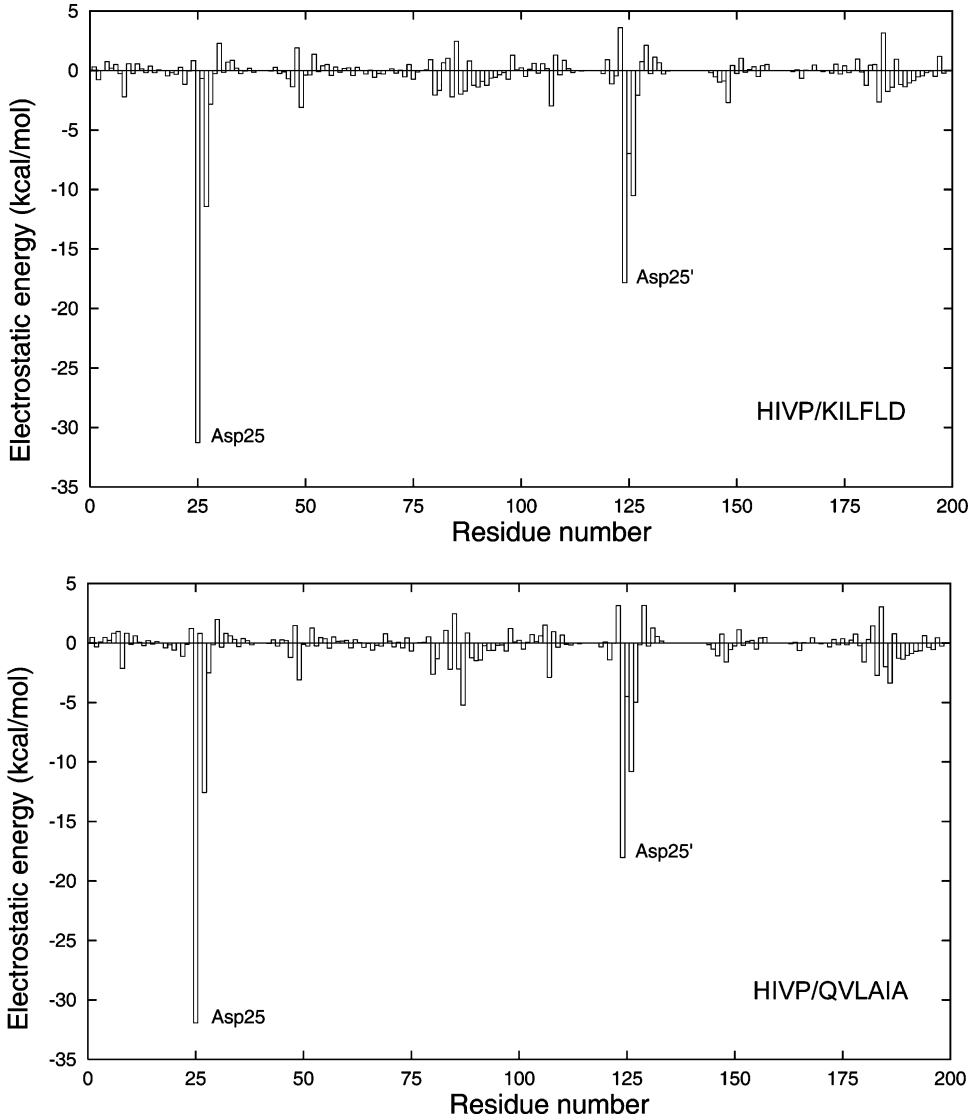

FIGURE 8: Electrostatic interactions between the residues in HIV-1 protease in complex with K-I-L-F-L-D (top) and Q-V-L-A-I-A (bottom) at the TI state, and the reacting system used in the EVB calculations.

results nor mutation studies (*16*) give any support to the hypothesis that the protein electric field is anticatalytic (*32*).

Linear Free Energy Relationships and Reorganization Energies. Differences in the so-called reorganization free energy between the water and enzyme reactions have also been shown to contribute significantly to enzymic rate accelerations (*54*, *72*−*74*). Recent simulations also showed that this effect manifests itself in the peptidyl transfer reaction on the ribosome (*75*). In a charge separation or transfer reaction taking place in aqueous solution, charge movement is followed by simultaneous reorientation of water dipoles leading to hydrogen bonds being broken and re-formed, which contributes significantly to the activation barrier. In enzymes, dipoles and charges may already be favorably orientated toward the transition state and the energy required to hold them at the correct orientation during catalysis is provided by the protein folding energy (*73*). This leads to a reduction of the reorganization energy, which can be considered a flattening of the reactant and product free energy curves with a concomitant reduction of the energy gap between them. The situation is illustrated schematically in Figure 9, for an elementary chemical step, where it can be appreciated that the intersection between the diabatic free energy curves is lowered as a consequence of reducing the reorganization energy, λ. Note that the depicted reorganiza-

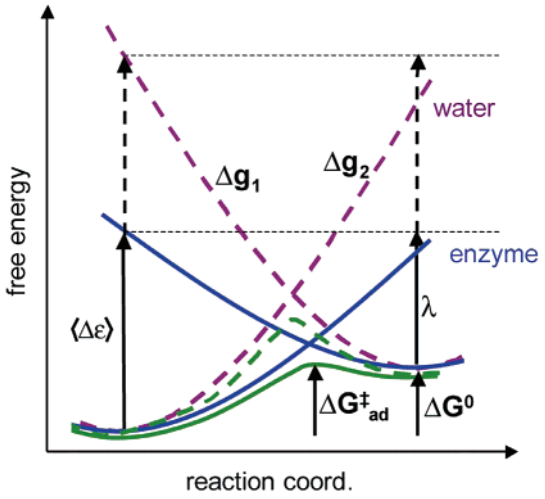

FIGURE 9: Reorganization energy λ as a function of the energy gap, $\langle\Delta\epsilon\rangle$, and the free energy difference for the reaction, ΔG°. Enzymes can lower the reorganization energy by changing the curvature of the diabatic free energy curves (Δg_1 and Δg_2).

tion energy corresponds to that of the product state and that an analogous λ can be defined for the reactant state. Reduction of either of the two reorganization energies (flattening of either of the two curves) will lower the free energy of the intersection point. Under the assumption of quadratic free energy functions, the relationship between activation and reaction free energy is given by Marcus formula (*76*)

$$\Delta G_{\mathrm{dia}}^{\ddagger} = \frac{(\Delta G_0 + \lambda)^2}{4\lambda} \quad (5)$$

Here, it should be emphasized that eq 5 pertains to the diabatic case with no mixing between the two states, of which electron transfer is the classical example (*76*). It is evident that for strongly adiabatic reactions, such as atom transfers with a large H_{12}, the use of eq 5 for deriving λ from experimental activation and reaction free energies will greatly underestimate the magnitude of λ, since the adiabatic curves are treated as if they were diabatic (*38*). Nevertheless, such a type of analysis is quite common (*76*−*79*) and can still yield useful predictions for different classes of reactions.

For adiabatic reactions, a change in $\Delta G°$ will also produce a change in activation free energy $\Delta G_{\mathrm{ad}}^{\ddagger}$ that approximately behaves according to eq 5, and this is why the simplified analysis using eq 5 can still work (although quantitatively underestimating the reorganization energy). The extension of Marcus formula to adiabatic reactions is, however, rather straightforward and can be written as (*80*)

$$\Delta G_{\mathrm{ad}}^{\ddagger} = \frac{(\Delta G_0 + \lambda)^2}{4\lambda} - \langle H_{12}(X^{\ddagger})\rangle_m + \frac{\langle H_{12}(X_{\mathrm{R}})\rangle_m{}^2}{\Delta G_0 + \lambda} \quad (6)$$

where the deviation of the adiabatic ground-state free energy from the diabatic situation now enters through the lowering of the energy due to quantum mechanical mixing both at the reactants [$H_{12}(X_{\mathrm{R}})$ term] and transition state [$H_{12}(X^{\ddagger})$ term].

Correlations between the activation free energy and the reaction free energy described by eqs 5 and 6 can appear to be linear within reasonable limits of $\Delta G°$ and are then known as linear free energy relationships (LFERs) as observed, e.g., in Brønsted plots. LFERs often provide a powerful empirical tool for analyzing chemical reactions, allowing predictions of the effects of changes in reaction free energy on the corresponding rates, and are well established for reactions involving smaller organic molecules (*81*). That enzymes also can follow the same type of relationships with respect to mutations or substrate modifications has been somewhat controversial (*82*), but different experimental and theoretical studies have demonstrated that this is the case (*14*, *38*, *79*, *83*−*86*). It should be noted here that the Marcus type of equations given above really only applies to elementary steps, and this is one reason why it is hard to apply this analysis to enzyme kinetic data, where rate constants and free energies associated with intermediates are notoriously difficult to obtain. The pioneering studies of Fersht and co-workers, however, examined the effect of enzyme mutations on equilibrium and rate constants for tyrosyl-tRNA synthetases and found significant linear relationships (*83*).

With the data from these calculations, it is of considerable interest to see whether different enzymes of the same family would also obey a LFER. We therefore used the calculated values of the activation and reaction free energies for the first reaction step leading to the transient tetrahedral intermediate in such an analysis, and the result is shown in Figure 10. It can immediately be seen that there is a clear correlation for the three enzymes, Plm II, Cat D, and HIVP (with two substrates), with a Brønsted β value of ~1. This thus implies that a change in the free energy of the tetrahedral intermediate has a very similar energetic effect on the transition state, which is, of course, in qualitative agreement with the Hammond postulate for the late TS. It can, however, be noted that the uncatalyzed water reaction does not fall on the same LFER as the three enzymes but lies 3−4 kcal/mol above it. This is clearly a manifestation of the reduced reorganization energy in the aspartic proteases, and a simplified analysis using eq 5 shows that the average calculated λ for the enzymes is 37 kcal/mol while it is 67 kcal/mol for the uncatalyzed reaction. As discussed above, using the standard Marcus treatment for adiabatic reactions considerably underestimates the calculated reorganization energy, and if we instead evaluate it directly from our calculated free energy functions, its magnitude becomes ~200 kcal/mol for the enzyme reactions but the reduction effect remains. The relatively large value of λ in this case is partly due to the fact that we are treating a concerted reaction path, which could, in principle, be divided into two elementary steps. Furthermore, it is worth noting that the calculated energetics of the HAP enzyme (*23*) does not fall on the aspartic protease LFER, which most likely reflects the difference in the catalytic groups.

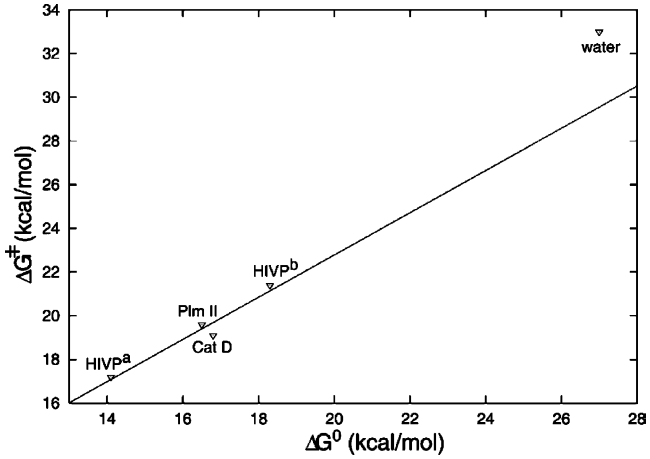

FIGURE 10: Linear free energy relationship for Plm II, Cat D, HIVP (a and b correspond to substrates K-I-L-F-L-D and Q-V-L-A-I-A, respectively), and the water reaction. Activation and reaction free energies for the first reaction step (Φ_1 to Φ_3) are plotted and correspond to the values given in Table 2.

The reduction of the reorganization free energy in enzymes is associated both with a preorganized catalytic active site conformation and with the relative rigidity of that structure. It has, however, recently been suggested that in HIVP it is the flexibility of the protein frame that is important and that conformational fluctuations play a major role for the catalytic effect by decreasing the free energy barrier (*30*, *32*). To address this issue, we repeated the calculations with the two HIVP substrates using atomic positional restraints of different strengths (10.0 and 100.0 kcal mol^{-1} Å^{-2}), applied to all heavy protein atoms except the two catalytic Asp side chains. The equilibrated enzyme structures generated earlier along

the reaction pathway (for the 41 FEP points) were used as references for the restraints in new FEP calculations. Relaxation of the enzyme along the reaction path is thus still retained, as the enzyme dipoles are still able to follow and stabilize the charge transfer during the reaction, while conformational fluctuations are seriously damped. The recalculated activation barriers are found to be virtually identical in these simulations, despite the fact that the effect of conformational fluctuations in catalysis is largely excluded. Although these calculations do not address the effect on the transmission coefficient for the reaction, they indicate that enzyme fluctuations, apart from motion along the reaction coordinate, do not have a major effect on the free energy barrier.

That some relaxation of enzyme dipoles along the reaction is indeed important can be seen by determining reaction profiles with restraints applied to only one reference structure throughout the whole FEP calculation. By restraining enzyme heavy atoms of HIVP/KILFLD by 10 kcal mol^{-1} $Å^{-2}$ as described above to the equilibrated conformation at the reactant minimum,we found the activation free energy to increase by ~5 kcal/mol. This is in agreement with ref *32*, in which the same effect was found. The contrary is observed if the restraints are applied with the TI structure as a reference, yielding a reduction of the activation barrier by ~4 kcal/mol. This implies that some degree of relaxation is essential during the reaction, since it involves movement of a negative charge, but the same is true also for the solution reaction. Since catalytic efficiency is an interplay between the binding of substrates and catalytic turnover, it is natural to assume that increasing the catalytic rate by rigidifying the enzyme in a conformation complementary to the TS or TI, as in the last example above, is going to have an opposite effect on binding. The significantly lower free energy barrier in such a rigidified enzyme is also accompanied by an additional reduction of the reorganization energy as expected (data not shown).

Hence, in contrast to refs *30* and *32*, we find no convincing support for the notion that the intrinsic enzyme conformational fluctuations contribute to the lowering of the free energy barrier. The fact that relaxation of the surroundings along the reaction coordinate is important is equally true for the uncatalyzed solution reaction and does not constitute a catalytic effect. Our results rather point to the importance of enzyme rigidity and the concomitant reduction of reorganization energy for catalysis, which is also in line with the fact that enzymes are always relatively large molecules. Of course, the ability of an enzyme to change its conformation is clearly important, e.g., in binding substrates, but this issue is quite separate from the proposal that intrinsic dynamic fluctuations contribute to stabilization of the transition states. At any rate, it seems clear that electrostatic stabilization, such as strong hydrogen bonding, is generally much more important for enhancing enzymic reaction rates than dynamic effects.

CONCLUDING REMARKS

We have analyzed the peptide hydrolysis reaction in aspartic proteases, with particular focus on the formation of the transient tetrahedral intermediate, using molecular dynamics simulations and the FEP/EVB method. The derived rate constants for the different six-amino acid substrates agree remarkably well with the experimental results. The quantitatively correct ranking of the two HIVP substrates is particularly encouraging. After establishing the validity of our simulations, we investigated the key interactions between the proteases and the tetrahedral intermediate. The replacement of serine and threonine residues, which interact with the outer Asp oxygens in Plm II and Cat D by alanines in HIVP, can be rationalized in terms of different pH optima, HIVP being active at higher pH. Furthermore, the strong interactions between the reacting groups and Gly27 in HIVP can partly compensate for these residues. It is also noteworthy that five structurally conserved water molecules in HIVP provide a significant stabilization of the tetrahedral intermediate and that, e.g., the absence of the Plm II/Cat D active site tyrosines does not render HIVP slower because of such compensating interactions. The structure−energy fingerprints (Figures 7 and 8) for the TI define the energetic characteristics of aspartic proteases but differ in details between PlmII/CatD and HIVP, demonstrating that it is the total effect of the enzyme (including bound water molecules) that matters. The high catalytic rate of aspartic proteases is thus mainly explained by the fact that the protein, together with structurally conserved water molecules, provides a three-dimensional network of dipoles favorably oriented for catalysis. This was also shown to be associated with a significant reduction of the reorganization free energy for the reaction. Furthermore, the stabilizing effect on the transition state and the tetrahedral intermediate is proportional as demonstrated by the calculated linear free energy relationship. Despite large structural differences between the studied aspartic proteases, they follow the same LFER and are capable of catalyzing peptide degradation at similar rates.

REFERENCES

1. Davies, D. R. (1990) The structure and function of the aspartic proteinases, *Annu. Rev. Biophys. Biophys. Chem. 19*, 189−215.
2. Fersht, A. (1999) *Structure and mechanism in protein science*, W. H. Freeman and Co., New York.
3. Dunn, B. M. (2002) Structure and mechanism of the pepsin-like family of aspartic peptidases, *Chem. Rev. 102*, 4431−4458.
4. Pearl, L., and Blundell, T. (1984) The active site of aspartic proteinases, *FEBS Lett. 174*, 96−101.
5. Suguna, K., Padlan, E. A., Smith, C. W., Carlson, W. D., and Davies, D. R. (1987) Binding of a reduced peptide inhibitor to the aspartic proteinase from *Rhizopus chinensis*: Implications for a mechanism of action, *Proc. Natl. Acad. Sci. U.S.A. 84*, 7009−7013.
6. Rodriguez, E. J., Angeles, T. S., and Meek, T. D. (1993) Use of nitrogen-15 kinetic isotope efects to elucidate details of the chemical mechanism of human imunodeficiency virus-1 potease, *Biochemistry 32*, 12380−12385.
7. Meek, T. D., Rodriguez, E. J., and Angeles, T. S. (1994) Use of Steady-State Kinetic Methods to Elucidate the Kinetic and Chemical Mechanisms of Retroviral Proteases, *Methods Enzymol. 241*, 127−156.
8. Brown, R. S., Bennet, A. J., and Slebocka-Tilk, H. (1992) Recent perspectives concerning the mechanism of H_3O^+- and OH^--promoted amide hydrolysis, *Acc. Chem. Res. 25*, 481−488.
9. Guthrie, J. P. (1974) Hydration of carboxamides. Evaluation of the free energy change for addition of water to acetamide and formamide derivatives, *J. Am. Chem. Soc. 96*, 3608−3615.
10. Bagno, A., Lovato, G., and Scorrano, G. (1993) Thermodynamics of protonation and hydration of aliphatic amides, *J. Chem. Soc., Perkin Trans. 2*, 1091−1098.
11. Veerapandian, B., Cooper, J. B., Sali, A., Blundell, T. L., Rosati, R. L., Dominy, B. W., Damon, D. B., and Hoover, D. J. (1992) Direct observation by X-ray analysis of the tetrahedral "intermediate" of aspartic proteinases, *Protein Sci. 1*, 322−328.

12. James, M. N. G., Sielecki, A. R., Hayakawa, K., and Gelb, M. H. (1992) Crystallographic analysis of transition-state mimics bound to penicillopepsin: Difluorostatine- and difluorostatone-containing peptides, *Biochemistry 31*, 3872−3886.
13. Northrop, D. B. (2001) Follow the protons: A low-barrier hydrogen bond unifies the mechanisms of the aspartic proteases, *Acc. Chem. Res. 34*, 790−797.
14. Warshel, A. (1991) *Computer modeling of chemical reactions in enzymes and solutions*, John Wiley & Sons, New York.
15. Åqvist, J., and Warshel, A. (1993) Simulation of enzyme-reactions using valence-bond force-fields and other hybrid quantum-classical approaches, *Chem. Rev. 93*, 2523−2544.
16. Loeb, D. D., Swanstrom, R., Everitt, L., Manchester, M., Stamper, S. E., and Hutchison, C. A., III (1989) Complete mutagenesis of the HIV-1 protease, *Nature 340*, 397−400.
17. Banerjee, R., Liu, J., Beatty, W., Pelosof, L., Klemba, M., and Goldberg, D. E. (2002) Four plasmepsins are active in the *Plasmodium falciparum* food vacuole, including a protease with an active-site histidine, *Proc. Natl. Acad. Sci. U.S.A. 99*, 990−995.
18. Ersmark, K., Feierberg, I., Bjelic, S., Hamelink, E., Hackett, F., Blackman, M. J., Hulten, J., Samuelsson, B., Åqvist, J., and Hallberg, A. (2004) Potent inhibitors of the *Plasmodium falciparum* enzymes plasmepsin I and II devoid of cathepsin D inhibitory activity, *J. Med. Chem. 47*, 110−122.
19. Ersmark, K., Nervall, M., Hamelink, E., Janka, L. K., Clemente, J. C., Dunn, B. M., Blackman, M. J., Samuelsson, B., Aqvist, J., and Hallberg, A. (2005) Synthesis of malarial plasmepsin inhibitors and prediction of binding modes by molecular dynamics simulations, *J. Med. Chem. 48*, 6090−6106.
20. Kohl, N. E., Emini, E. A., Schleif, W. A., Davis, L. J., Heimbach, J. C., Dixon, R. A. F., Scolnick, E. M., and Sigal, I. S. (1988) Active human immunodeficiency virus protease is required for viral infectivity, *Proc. Natl. Acad. Sci. U.S.A. 85*, 4686−4690.
21. Brik, A., and Wong, C. H. (2003) HIV-1 protease: Mechanism and drug discovery, *Org. Biomol. Chem. 1*, 5−14.
22. Strajbl, M., Florian, J., and Warshel, A. (2000) Ab initio evaluation of the potential surface for general base-catalyzed methanolysis of formamide: A reference solution reaction for studies of serine proteases, *J. Am. Chem. Soc. 122*, 5354−5366.
23. Bjelic, S., and Aqvist, J. (2004) Computational prediction of structure, substrate binding mode, mechanism, and rate for a malaria protease with a novel type of active site, *Biochemistry 43*, 14521−14528.
24. Ishida, T., and Kato, S. (2003) Theoretical perspectives on the reaction mechanism of serine proteases: The reaction free energy profiles of the acylation process, *J. Am. Chem. Soc. 125*, 12035−12048.
25. Kaminski, Z. J., Paneth, P., and Oleary, M. H. (1991) Nitrogen kinetic isotope effects on the acylation of aniline, *J. Org. Chem. 56*, 5716−5718.
26. Sawyer, C. B., and Kirsch, J. F. (1973) Kinetic isotope effects for reactions of methyl formate-*methyloxy*-$^{18}O^{1}$, *J. Am. Chem. Soc. 95*, 7375−7381.
27. Yang, C. C., and Jencks, W. P. (1988) The aminolysis of methyl formate with aniline: Evidence for catalysis by a trapping mechanism, *J. Am. Chem. Soc. 110*, 2972−2973.
28. Hyland, L. J., Tomaszek, T. A., and Meek, T. D. (1991) Human immunodeficiency virus-1 protease. 2. Use of pH rate studies and solvent kinetic isotope effects to elucidate details of chemical mechanism, *Biochemistry 30*, 8454−8463.
29. Hyland, L. J., Tomaszek, T. A., Roberts, G. D., Carr, S. A., Magaard, V. W., Bryan, H. L., Fakhoury, S. A., Moore, M. L., Minnich, M. D., Culp, J. S., Desjarlais, R. L., and Meek, T. D. (1991) Human immunodeficiency virus-1 protease. 1. Initial velocity studies and kinetic characterization of reaction intermediates by ^{18}O isotope exchange, *Biochemistry 30*, 8441−8453.
30. Cascella, M., Micheletti, C., Rothlisberger, U., and Carloni, P. (2005) Evolutionarily conserved functional mechanics across pepsin-like and retroviral aspartic proteases, *J. Am. Chem. Soc. 127*, 3734−3742.
31. Chatfield, D. C., Eurenius, K. P., and Brooks, B. R. (1998) HIV-1 protease cleavage mechanism: A theoretical investigation based on classical MD simulation and reaction path calculations using a hybrid QM/MM potential, *THEOCHEM 423*, 79−92.
32. Piana, S., Bucher, D., Carloni, P., and Rothlisberger, U. (2004) Reaction mechanism of HIV-1 protease by hybrid Car-Parrinello/classical MD simulations, *J. Phys. Chem. B 108*, 11139−11149.
33. Trylska, J., Grochowski, P., and McCammon, J. A. (2004) The role of hydrogen bonding in the enzymatic reaction catalyzed by HIV-1 protease, *Protein Sci. 13*, 513−528.
34. Luzhkov, V., and Åqvist, J. (1998) Computer simulation of phenyl ester cleavage by β-cyclodextrin in solution, *J. Am. Chem. Soc. 120*, 6131−6137.
35. Zwanzig, R. W. (1954) High-temperature equation of state by a perturbation method. I. Nonpolar gases, *J. Chem. Phys. 22*, 1420−1426.
36. Eigen, M. (1964) Proton transfer, acid−base catalysis, and enzymatic hydrolysis. Part I: Elementary processes, *Angew. Chem., Int. Ed. 3*, 1−72.
37. Deraniyagala, S. A., Adediran, S. A., and Pratt, R. F. (1995) β-Secondary and solvent deuterium kinetic isotope effects and the mechanisms of base-catalyzed and acid-catalyzed hydrolysis of penicillanic acid, *J. Org. Chem. 60*, 1619−1625.
38. Åqvist, J. (1997) Modelling of proton-transfer reactions in enzymes, in *Computational approaches to biochemical reactivity* (Náray-Szabó, G., and Warshel, A., Eds.) pp 341−362, Kluwer Academic Publishers, Dordrecht, The Netherlands.
39. Slebocka-Tilk, H., Neverov, A. A., and Brown, R. S. (2003) Proton inventory study of the base-catalyzed hydrolysis of formamide. Consideration of the nucleophilic and general base mechanisms, *J. Am. Chem. Soc. 125*, 1851−1858.
40. Asojo, O. A., Afonina, E., Gulnik, S. V., Yu, B., Erickson, J. W., Randad, R., Medjahed, D., and Silva, A. M. (2002) Structures of Ser205 mutant plasmepsin II from *Plasmodium falciparum* at 1.8 angstrom in complex with the inhibitors rs367 and rs370, *Acta Crystallogr. D58*, 2001−2008.
41. Baldwin, E. T., Bhat, T. N., Gulnik, S., Hosur, M. V., Sowder, R. C., Cachau, R. E., Collins, J., Silva, A. M., and Erickson, J. W. (1993) Crystal structures of native and inhibited forms of human cathepsin D: Implications for lysosomal targeting and drug design, *Proc. Natl. Acad. Sci. U.S.A. 90*, 6796−6800.
42. Miller, M., Schneider, J., Sathyanarayana, B. K., Toth, M. V., Marshall, G. R., Clawson, L., Selk, L., Kent, S. B. H., and Wlodawer, A. (1989) Structure of complex of synthetic HIV-1 protease with a substrate-based inhibitor at 2.3 Å resolution, *Science 246*, 1149−1152.
43. Rodriguez, E. J., Debouck, C., Deckman, I. C., Abusoud, H., Raushel, F. M., and Meek, T. D. (1993) Inhibitor binding to the Phe53Trp mutant of HIV-1 protease promotes conformational changes detectable by spectrofluorometry, *Biochemistry 32*, 3557−3563.
44. Boross, P., Bagossi, P., Copeland, T. D., Oroszlan, S., Louis, J. M., and Tozser, J. (1999) Effect of substrate residues on the P2′ preference of retroviral proteinases, *Eur. J. Biochem. 264*, 921−929.
45. Pimenta, D. C., Oliveira, A., Juliano, M. A., and Juliano, L. (2001) Substrate specificity of human cathepsin D using internally quenched fluorescent peptides derived from reactive site loop of kallistatin, *Biochim. Biophys. Acta 1544*, 113−122.
46. Istvan, E. S., and Goldberg, D. E. (2005) Distal substrate interactions enhance plasmepsin activity, *J. Biol. Chem. 280*, 6890−6896.
47. Jorgensen, W. L., Chandrasekhar, J., and Madura, J. D. (1983) Comparison of simple potential functions for simulating liquid water, *J. Chem. Phys. 79*, 926−935.
48. Marelius, J., Kolmodin, K., Feierberg, I., and Åqvist, J. (1998) Q: A molecular dynamics program for free energy calculations and empirical valence bond simulations in biomolecular systems, *J. Mol. Graphics 16*, 213−225.
49. Jorgensen, W. L., Maxwell, D. S., and TiradoRives, J. (1996) Development and testing of the OPLS all-atom force field on conformational energetics and properties of organic liquids, *J. Am. Chem. Soc. 118*, 11225−11236.
50. Lee, F. S., and Warshel, A. (1992) A local reaction field method for fast evaluation of long-range electrostatic interactions in molecular simulations, *J. Chem. Phys. 97*, 3100−3107.
51. King, G., and Warshel, A. (1989) A surface constrained all-atom solvent model for effective simulations of polar solutions, *J. Chem. Phys. 91*, 3647−3661.
52. Ryckaert, J. P., Ciccotti, G., and Berendsen, H. J. C. (1977) Numerical integration of the Cartesian equations of motion of a system with constraints: Molecular dynamics of *n*-alkanes, *J. Comput. Phys. 23*, 327−341.
53. Siripurkpong, P., Yuvaniyama, J., Wilairat, P., and Goldberg, D. E. (2002) Active site contribution to specificity of the aspartic proteases plasmepsins I and II, *J. Biol. Chem. 277*, 41009−41013.

54. Feierberg, I., and Åqvist, J. (2002) Computational modeling of enzymatic keto−enol isomerization reactions, *Theor. Chem. Acc. 108*, 71−84.
55. Blundell, T. L., Cooper, J., Foundling, S. I., Jones, D. M., Atrash, B., and Szelke, M. (1987) On the rational design of renin inhibitors: X-ray studies of aspartic proteinases complexed with transition-state analogues, *Biochemistry 26*, 5585−5590.
56. Fraser, M. E., Strynadka, N. C. J., Bartlett, P. A., Hanson, J. E., and James, M. N. G. (1992) Crystallographic analysis of transition-state mimics bound to penicillopepsin: Phosphorus-containing peptide analogs, *Biochemistry 31*, 5201−5214.
57. Coates, L., Erskine, P. T., Crump, M. P., Wood, S. P., and Cooper, J. B. (2002) Five atomic resolution structures of endothiapepsin inhibitor complexes: Implications for the aspartic proteinase mechanism, *J. Mol. Biol. 318*, 1405−1415.
58. Smith, R., Brereton, I. M., Chai, R. Y., and Kent, S. B. H. (1996) Ionization states of the catalytic residues in HIV-1 protease, *Nat. Struct. Biol. 3*, 946−950.
59. Porter, D. J. T., Hanlon, M. H., and Furfine, E. S. (2002) HIV-1 protease: Characterization of a catalytically competent enzyme−substrate intermediate, *Biochemistry 41*, 1302−1307.
60. Bigeleisen, J., and Mayer, M. G. (1947) Calculation of equilibrium constants for isotopic exchange reactions, *J. Chem. Phys. 15*, 261−267.
61. Gawlita, E., Lantz, M., Paneth, P., Bell, A. F., Tonge, P. J., and Anderson, V. E. (2000) H-Bonding in alcohols is reflected in the Cα-H bond strength: Variation of C−D vibrational frequency and fractionation factor, *J. Am. Chem. Soc. 122*, 11660−11669.
62. Kolmodin, K., Luzhkov, V. B., and Åqvist, J. (2002) Computational study of the influence of solvent on O-16/O-18 equilibrium isotope effects in phosphate deprotonation reactions, *J. Am. Chem. Soc. 124*, 10130−10135.
63. Okoniewska, M., Tanaka, T., and Yada, R. Y. (1999) The role of the flap residue, threonine 77, in the activation and catalytic activity of pepsin A, *Protein Eng. 12*, 55−61.
64. Tong, L. A., Pav, S., Lamarre, D., Simoneau, B., Lavallee, P., and Jung, G. (1995) Crystallographic studies on the binding modes of P-2-P-3 butanediamide renin inhibitors, *J. Biol. Chem. 270*, 29520−29524.
65. Andreeva, N. S., and Rumsh, L. D. (2001) Analysis of crystal structures of aspartic proteinases: On the role of amino acid residues adjacent to the catalytic site of pepsin-like enzymes, *Protein Sci. 10*, 2439−2450.
66. Francis, S. E., Sullivan, D. J., and Goldberg, D. E. (1997) Hemoglobin metabolism in the malaria parasite *Plasmodium falciparum*, *Annu. Rev. Microbiol. 51*, 97−123.
67. Reichelt, D., Jacobsohn, E., and Haschen, R. J. (1974) Purification and properties of cathepsin D from human erythrocytes, *Biochim. Biophys. Acta 341*, 15−26.
68. Mahalingam, B., Louis, J. M., Hung, J., Harrison, R. W., and Weber, I. T. (2001) Structural implications of drug-resistant mutants of HIV-1 protease: High-resolution crystal structures of the mutant protease/substrate analogue complexes, *Proteins 43*, 455−464.
69. Bakowies, D., and Kollman, P. A. (1999) Theoretical study of base-catalyzed amide hydrolysis: Gas- and aqueous-phase hydrolysis of formamide, *J. Am. Chem. Soc. 121*, 5712−5726.
70. Thomas, K. A., Smith, G. M., Thomas, T. B., and Feldmann, R. J. (1982) Electronic distributions within protein phenylalanine aromatic rings are reflected by three-dimensional oxygen atom environments, *Proc. Natl. Acad. Sci. U.S.A. 79*, 4843−4847.
71. Park, Y. N., Aikawa, J., Nishiyama, M., Horinouchi, S., and Beppu, T. (1996) Involvement of a residue at position 75 in the catalytic mechanism of a fungal aspartic proteinase, *Rhizomucor pusillus* pepsin. Replacement of tyrosine 75 on the flap by asparagine enhances catalytic efficiency, *Protein Eng. 9*, 869−875.
72. Åqvist, J., and Fothergill, M. (1996) Computer simulation of the triosephosphate isomerase catalyzed reaction, *J. Biol. Chem. 271*, 10010−10016.
73. Warshel, A. (1978) Energetics of enzyme catalysis, *Proc. Natl. Acad. Sci. U.S.A. 75*, 5250−5254.
74. Yadav, A., Jackson, R. M., Holbrook, J. J., and Warshel, A. (1991) Role of solvent reorganization energies in the catalytic activity of enzymes, *J. Am. Chem. Soc. 113*, 4800−4805.
75. Trobro, S., and Åqvist, J. (2005) Mechanism of peptide bond synthesis on the ribosome, *Proc. Natl. Acad. Sci. U.S.A. 102*, 12395−12400.
76. Marcus, R. A. (1964) Chemical and electrochemical electron-transfer theory, *Annu. Rev. Phys. Chem. 15*, 155−196.
77. Albery, W. J. (1980) The application of the Marcus relation to reactions in solution, *Annu. Rev. Phys. Chem. 31*, 227−263.
78. Cannon, W. R., and Benkovic, S. J. (1998) Solvation, reorganization energy, and biological catalysis, *J. Biol. Chem. 273*, 26257−26260.
79. Silverman, D. N., Tu, C. K., Chen, X., Tanhauser, S. M., Kresge, A. J., and Laipis, P. J. (1993) Rate-equilibria relationships in intramolecular proton transfer in human carbonic anhydrase III, *Biochemistry 32*, 10757−10762.
80. Warshel, A., Hwang, J. K., and Åqvist, J. (1992) Computer simulations of enzymatic reactions: Examination of linear free-energy relationships and quantum-mechanical corrections In the initial proton-transfer step of carbonic-anhydrase, *Faraday Discuss.*, 225−238.
81. Wiberg, K. B. (1964) *Physical organic chemistry*, John Wiley & Sons, New York.
82. Straub, J. E., and Karplus, M. (1990) The interpretation of site-directed mutagenesis experiments by linear free energy relations, *Protein Eng. 3*, 673−675.
83. Fersht, A. R., Leatherbarrow, R. J., and Wells, T. N. C. (1987) Structure−activity relationships in engineered proteins: Analysis of use of binding energy by linear free energy relationships, *Biochemistry 26*, 6030−6038.
84. Toney, M. D., and Kirsch, J. F. (1989) Direct Brönsted analysis of the restoration of activity to a mutant enzyme by exogenous amines, *Science 243*, 1485−1488.
85. Warshel, A., Schweins, T., and Fothergill, M. (1994) Linear free energy relationships in enzymes. Theoretical analysis of the reaction of tyrosyl-tRNA synthetase, *J. Am. Chem. Soc. 116*, 8437−8442.
86. Schutz, C. N., and Warshel, A. (2004) Analyzing free energy relationships for proton translocations in enzymes: Carbonic anhydrase revisited, *J. Phys. Chem. B 108*, 2066−2075.
87. Asojo, O. A., Gulnik, S. V., Afonina, E., Yu, B., Ellman, J. A., Haque, T. S., and Silva, A. M. (2003) Novel uncomplexed and complexed structures of plasmepsin II, an aspartic protease from *Plasmodium falciparum*, *J. Mol. Biol. 327*, 173−181.
88. Goldblum, A. (1988) Theoretical calculations on the acidity of the active-site in aspartic proteinases, *Biochemistry 27*, 1653−1658.
89. Silva, A. M., Cachau, R. E., Sham, H. L., and Erickson, J. W. (1996) Inhibition and catalytic mechanism of HIV-1 aspartic protease, *J. Mol. Biol. 255*, 321−340.
90. Park, H., Suh, J., and Lee, S. (2000) Ab initio studies on the catalytic mechanism of aspartic proteinases: Nucleophilic versus general acid/general base mechanism, *J. Am. Chem. Soc. 122*, 3901−3908.

BI060131Y